Iodoethylammonium (IEA+)-based lead- and iodide-deficient halide perovskites (d-HPs) for solar cells

Thierry Pauporté, Liam Gollino, Nicolas Mercier

Please cite this paper as : T. Pauporté, L. Gollino, N. Mercier, Ethylammonium (IEA+)-based lead- and iodide- deficient halide perovskites (d-HPs) for solar cells. Proc. SPIE, 12422 (2023) 124220M. https://doi.org/10.1117/12.2647859

Iodoethylammonium (IEA^+)-based lead- and iodide- deficient halide perovskites (d-HPs) for solar cells

T. Pauporté*[a], L. Gollino[a], N. Mercier[b]

[a]Chimie ParisTech, PSL Université, CNRS, Institut de Recherche de ChimieParis (IRCP), UMR8247, 11 rue Pierre et Marie Curie, F-75231 Paris cedex 05, France
[b]University of Angers, MOLTECH-ANJOU, UMR6200, 2 boulevard de Lavoisier, 49045 Angers
*Email: thierry.pauporte@chimieparistech.psl.eu

ABSTRACT

Perovskite materials, despite displaying remarkable properties, suffer from the use of toxic lead and poor stability towards moisture and thermal stresses. These strongly hinder their future development. Recently, a new family of 3D perovskites, deficient in lead and iodide, the d-HPs, has been discovered. They involve large organic cations that circumvent the Goldschmidt tolerance factor. In the present study, we report that a new cation, the iodoethylammonium $I\text{-}(CH_2)_2\text{-}NH_3^+$ (IEA^+), allows the synthesis of d-HP thin films based on the 3D $MAPbI_3$ perovskite. This new compound has been tested for solar cell application. A final power conversion efficiency of 9.54 % was achieved.

Keywords: Perovskite solar cells, Lead- and iodide-Deficient perovskite, Iodoethylammonium, $MAPbI_3$, toxicity

1. INTRODUCTION

Hybrid halide perovskites (PVK) are promising semiconductors studied for numerous applications due to their various interesting optoelectronic properties such as high charge carrier mobility, tunable bandgap, high absorption coefficient, long carriers diffusion lengths and low recombination losses [1–6]. Their possible applications encompass notably lasers [7], LEDs [8], photodetectors [9,10] scintillation [11] and perovskite solar cells (PSCs) [12–17]. PSCs have become more and more attractive and investigated, with nowadays a record power conversion efficiency (PCE) of 25.7% [18] that competes directly with the commercialized silicon photovoltaic solar cells [19]. Nevertheless, perovskites faces two major issues: a rather poor stability [20,21] as well as a high toxicity caused by the presence of lead [22,23]. To solve them, one method is to replace lead totally or partially by other elements [24–26]. In recent years, we reported the d-HPs (Lead -and iodide-Deficient Halide Perovskites), a new family of 3D perovskites with an original structure presenting PbI^+ vacancies inside the perovskite lattice caused by the insertion of large organic cations that do not respect the Goldschmidt tolerance factor. Two large organic cations have been reported so far: hydroxyethylammonium, $HO\text{-}(CH_2)_2\text{-}NH_3^+$ (noted HEA^+)[27] and thioethylammonium, $HS\text{-}(CH_2)_2\text{-}NH_3^+$ (noted TEA^+) [28]. By inserting these cations, lead- and iodide- deficient $MAPbI_3$ (MAPI) and $FAPbI_3$ (FAPI) have been obtained with 3D corned-shared $Pb_{1-x}I_{3-x}$ network and which display an impressively enhanced stability alongside a reduced toxicity.

In the present work, we unveil the use of the large organic cation iodoethylammonium $I\text{-}(CH_2)_2\text{-}NH_3^+$ (noted IEA^+) to successfully synthetize the lead- and iodide- deficient $MAPbI_3$, noted d-MAPI-IEA, as thin films. They have been characterized by X-Ray Diffraction (XRD) and UV-Visible absorbance measurements. The resulting d-HP films have been additionally characterized by Scanning Electron Microscopy (SEM) and time-resolved photoluminescence (TRPL) to assess the impact of PbI^+ units octahedra substitution by IEA^+ on the optoelectronic and morphological properties of the perovskite layer. Finally, d-MAPI-IEA thin films have been incorporated in operational FTO/c-TiO_2/m-

Please cite this paper as : T. Pauporté, L. Gollino, N. Mercier, Ethylammonium (IEA+)-based lead- and iodide- deficient halide perovskites (d-HPs) for solar cells. Proc. SPIE, 12422 (2023) 124220M. https://doi.org/10.1117/12.2647859

TiO_2/PVK/spiro-OMeTAD/Au PSC structure (with c-TiO_2 a compact TiO_2 layer and m-TiO_2 a mesoporous TiO_2 layer) to prove the feasibility of such photovoltaic devices and a final efficiency of 9.54 % was achieved.

2. EXPERIMENTAL SECTION

Fluorine-doped SnO_2 (FTO) substrates (TEC 7 from Pilkington) were etched pattern by zinc oxide powder and 10 % HCl solution prior to be cleaned with soap and water. The substrates were subsequently plunged for 20 min in a concentrated 2.2 M NaOH in ethanol/water (10:1 volume ratio) and cleaned in acetone using an ultrasonic bath for 12 min. They were then rinsed with deionized water in an ultrasonic bath for 15 min.[29] The substrates were subsequently heated at 500 °C for 15 min. The compact TiO_2 electron transporting layer (ETL), noted c-TiO_2, was prepared by aerosol spray pyrolysis as detailed in Ref. [30]. The anatase TiO_2 NR30-D paste (from Greatcell Solar Materials) was diluted in ethanol with a 1:7 w/w ratio. 45 µL of the solution was dropped onto the compact TiO_2 layer and spin-coated at 2000 rpm for 15 s. The layer was then dried on a hotplate at 70 °C for at least 10 min and finally heated at 500 °C under an air flux for 30 min, cooled down to 200 °C and removed from the hotplate before being transferred immediately to a N_2-filled glovebox for perovskite layer deposition.

The perovskite layers were deposited using a one-step spin-coating method. For the $MAPbI_3$ layer, a perovskite precursor solution with a concentration of 1.35 M was prepared by mixing 214.6 mg of MAI (Greatcell Solar Materials) and 622.3 mg of PbI_2 (TCI) in 1 mL of DMSO. The solution, placed in a tightly closed bottle, was stirred for 2 h at 100 °C in a N_2-filled glovebox. 40 µL of this solution was placed on top of the substrate before starting the spin-coating in a N_2-filled glovebox. The spinning routine used was: 1000 rpm with an acceleration of 200 rpm/s for 10 s followed by a second spinning at 6000 rpm for 30 s with an acceleration of 4000 rpm/s. 100 µL of chlorobenzene was dripped 30 s after the start of the spinning routine at a slow speed. The films were then annealed on a hotplate at 105 °C for 1h inside a N_2 filled glovebox.

For the d-MAPI-IEA, a perovskite precursor solution with a concentration of 1.0 M was prepared by mixing 132.5 mg of MAI (Greatcell Solar Materials), 384.2 mg of PbI_2 (TCI) and 176.3 mg of $(IEA)_2PbI_4$ (n=1 $MAPbI_3$-IEAI precursor) in 1 mL of DMF. The solution, placed in a tightly closed bottle, was stirred for 3 h at 50 °C in a N_2-filled glovebox. 40 µL of this solution was placed on the top of the substrate before starting the spin-coating in a N_2-filled glovebox. The spinning routine used was: 1000 rpm with an acceleration of 500 rpm/s for 10 s followed by a second spinning at 5000 rpm for 30 s with an acceleration of 1500 rpm/s. 100 µL of chlorobenzene was dripped 15 s after the start of the spinning routine at slow speed. The films were finally annealed at 150 °C for 1 hour. To finish the cells, a Spiro-OMeTAD layer was spin-coated and a gold back contact electrode was thermally evaporated as described in Ref. [30].

Perovskite film structure was characterized using a PANanalytical X-Pert high-resolution XRD operated at 40 kV and 45 mA and using the Cu Kα radiation with λ = 1.5406 Å. The film specular absorbance was measured by a Cary 5000 UV–vis–NIR spectrophotometer using an integrating sphere. A glass/FTO/c-TiO_2/m-TiO_2 sample was used for the baseline. The time-resolved photoluminescence (TRPL) measurements were performed under a microscope lens (numerical aperture 0.7). The perovskites layers were spin-coated onto a glass/FTO/c-TiO_2/m-TiO_2 substrate. The top of the PVK layer was excited by a 470 nm diode laser (Picoquant) filtered by a 488 nm long pass filter. The emission was analyzed for TRPL decay by a PerkinElmer SPCM avalanche photodiode combined with a Picoharp acquisition card (500 ps characteristic time of the total system response function) used with the laser in a pulsed mode at a 10 nW excitation power (pulse duration 70 ps). The solar cells *J–V* curves were recorded by a Keithley 2410 digital source meter, using a 0.1 $V.s^{-1}$ voltage scan rate. The solar cells were illuminated with a solar simulator (Abet Technology Sun 2000) filtered to mimic AM 1.5G conditions (100 mW cm^{-2}). The illuminated surface was delimited by a black mask with an aperture diameter of 3 mm. The power density was calibrated at 100 mW cm^{-2} by the use of a reference silicon solar cell.

3. RESULTS AND DISCUSSION

All the perovskite solar cells depicted here were fabricated using a direct mesoporous architecture consisting of an FTO-coated glass as substrates, a combination c-TiO_2 and m-TiO_2 layers as electron transporting layer (ETL), perovskite (PVK) as the absorber, Spiro-OMeTAD as hole transporting layer (HTL) and gold as counter-electrode (**Figure 1a**). The d-HP presently studied consists in a classic 3D $MAPbI_3$ in which we substituted PbI^+ units by iodoethylammonium

Please cite this paper as : T. Pauporté, L. Gollino, N. Mercier, Ethylammonium (IEA+)-based lead- and iodide- deficient halide perovskites (d-HPs) for solar cells. Proc. SPIE, 12422 (2023) 124220M. https://doi.org/10.1117/12.2647859

(IEA^+) large organic cation. A schematic representation of the crystallographic structure of the classic 3D $MAPbI_3$ and the resulting d-MAPI-IEA is shown in **Figure 1b**. Both systems were thoroughly investigated and optimized.

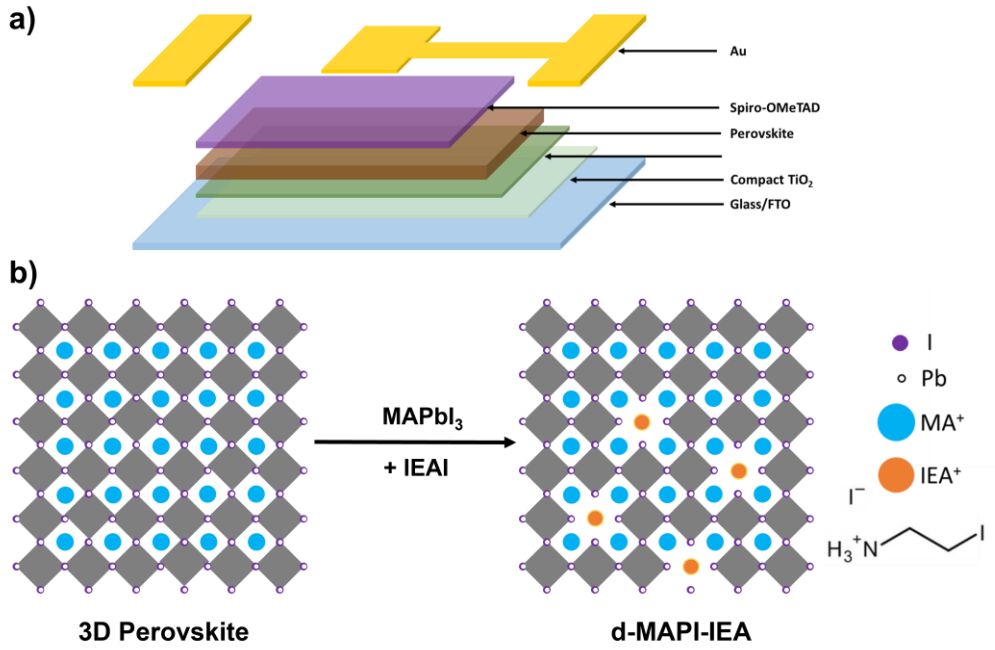

Figure 1: (a) Exploded schematic view of the perovskite solar cell structure. (b) Schematic representation of classic 3D $MAPbI_3$ and of 3D d-MAPI-IEA perovskite formed after partial substitution of PbI^+ units by IEA^+ cations.

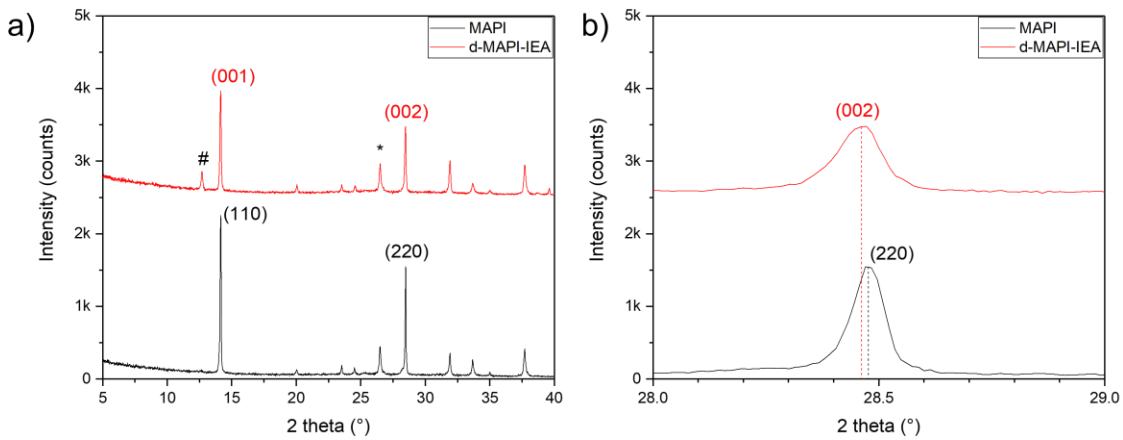

Figure 2: (a) XRD patterns of $MAPbI_3$ and d-MAPI-IEA perovskite films (FTO peaks are indicated by *. # symbol represents PbI_2) (b) Same as (a) zoomed between 28-29°.

X-Ray diffractions patterns depicted in **Figure 2a** show a slight reduction of the perovskite (001) and (002) peaks of the d-MAPI-IEA compared to its classic $MAPbI_3$ (110) and (220) analogues. Also, a non-negligeable PbI_2 peak at 12.7° is present for d-MAPI-IEA. These elements suggest a lower crystallinity of the perovskite caused by the IEA^+ cations insertion within the $MAPbI_3$ lattice to form the d-HP. In **Figure 2b**, a shift of the Bragg reflections to smaller 2θ angles

Please cite this paper as : T. Pauporté, L. Gollino, N. Mercier, Ethylammonium (IEA+)-based lead- and iodide- deficient halide perovskites (d-HPs) for solar cells. Proc. SPIE, 12422 (2023) 124220M. https://doi.org/10.1117/12.2647859

for d-MAPI-IEA, indicates an expansion of the unit cell. This expansion proves the good insertion of IEA^+ within the $MAPbI_3$ lattice and thus the correct formation of the d-MAPI-IEA compound as described and proved for other few systems in the past by our groups [27,28].

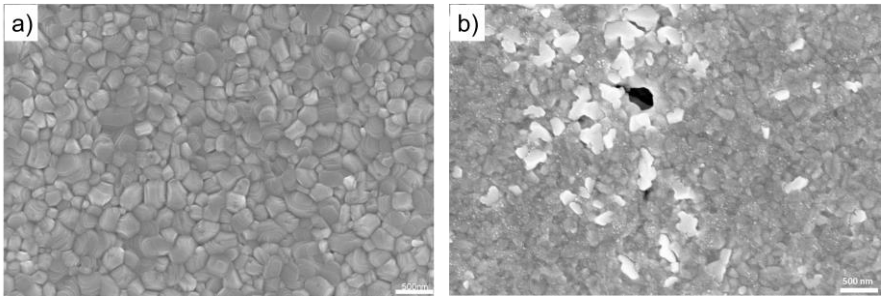

Figure 3: Top-view SEM of (a) $MAPbI_3$ and (b) d-MAPI-IEA perovskite films. Scale bar: 500 nm.

Top-view SEM images were obtained to assess the morphology of the d-MAPI-IEA film. The film presents important pinholes (**Figure 3b**) and PbI_2 flakes (white flakes) which are not observed for the $MAPbI_3$ film (**Figure 3a**). Furthermore, the d-MAPI-IEA film is constituted of rather small grains. These facts agree with the reduced crystallinity and the PbI_2 peak observed previously on the XRD patterns (**Figure 2**). The presence of IEA^+ thus causes a consequent downgrading of the perovskite morphology that will be shown to greatly hinder the devices efficiency and the potential of this d-HP for photovoltaic applications.

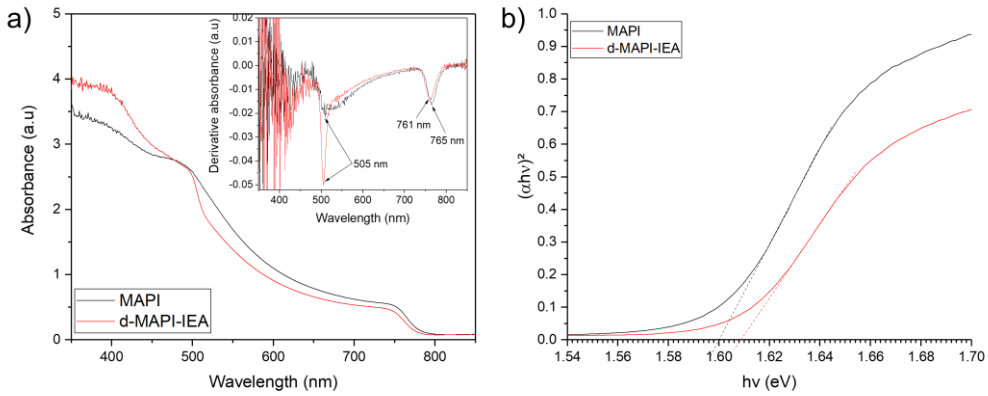

Figure 4: (a) UV-Visible spectra of $MAPbI_3$ and d-MAPI-IEA perovskite films. Inset: the associated derivative absorbance. (b) Tauc Plot associated to the UV-Visible absorbance spectra.

The UV-Visible absorbance spectrum of the optimized d-MAPI-IEA film was measured and compared to the reference $MAPbI_3$ (**Figure 4a**). The two films presented an absorbance edge in the 760-770 nm range. An additional edge at 505 nm was clearly observed after IEA^+ insertion, causing the d-MAPI-IEA to have a better absorbance below 505 nm. For a similar d-HP, the d-MAPI-HEA, a comparable edge was found at 555 nm and was attributed to the presence of domains with a high substitution level of PbI^+ by HEA^+ which cause the perovskite film to become slightly reddish.[27] In the case of d-MAPI-IEA, the same trend is observed. Indeed, as the content of IEA^+ within the lattice increases, the perovskite layer becomes red (**Figure 5**). In our case, despite the low substitution level of PbI^+ by IEA^+ used, domains with important substitution rate could exist and explain the presence of the absorbance edge at 505 nm. All over the rest of the UV-Visible region, the d-MAPI-IEA displays an inferior absorbance, which counteracts the beneficial aforementioned effect. The derivative absorbance highlights a slight blue-shift of the absorption edge around 760-770 nm, caused by

Please cite this paper as : T. Pauporté, L. Gollino, N. Mercier, Ethylammonium (IEA+)-based lead- and iodide- deficient halide perovskites (d-HPs) for solar cells. Proc. SPIE, 12422 (2023) 124220M. https://doi.org/10.1117/12.2647859

direct optical transition in the metal-organic perovskite absorber. We confirmed this blue-shift by plotting the Tauc plot of the absorbance spectra (**Figure 4b**). This allowed us to extract the optical bandgap values of $MAPbI_3$ and d-MAPI-IEA perovskites at 1.60 eV and 1.61 eV, respectively. Such an increase of the bandgap value was expected with the expansion of the unit cell volume caused by IEA^+ cations insertion within the perovskite lattice and conclude the proof of formation of the d-HP d-MAPI-IEA.

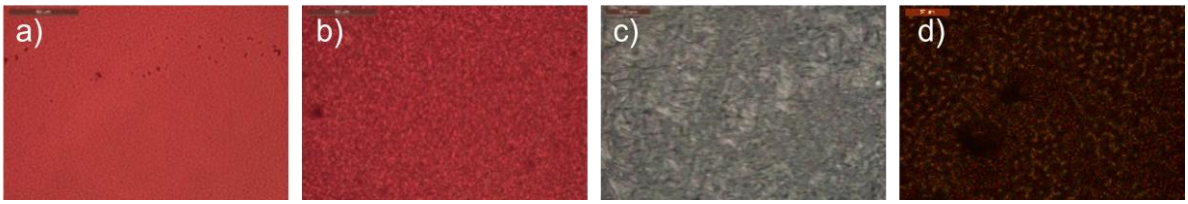

Figure 5: Optical microscope pictures of d-MAPI-IEA films for Pb/MA/IEA molar ratios of (a) 1/0.5/1 (b) 1/0.66/0.66 (c) 1/0.75/0.5 and (d) 1/0.8/0.4 (IEA^+ content decreases from a) to d))

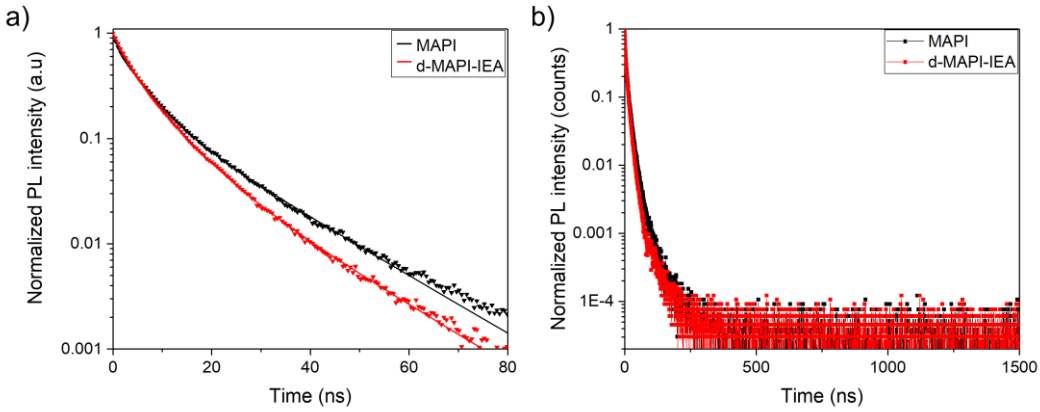

Figure 6: Normalized time-resolved photoluminescence of $MAPbI_3$ and d-MAPI-IEA films on FTO/c-TiO_2/m-TiO_2 substrates. (a) Zoom between 0-80 ns. (b) Measurement over 1500 ns. The full lines are the fitting curves obtained from the triple exponential fitting of the experimental points (downward triangles).

Table 1: Exponential function for TRPL fitting and extracted parameters

ExpDec3 : $y = y_0 + A_1 \exp(-t/\tau_1) + A_2 \exp(-t/\tau_2) + A_3 \exp(-t/\tau_3)$							
Sample	y_0	A_1	τ_{fast}	A_2	τ_{int}	A_3	τ_{slow}
$MAPbI_3$	4.14E-5	0.19	0.72	0.58	5.00	0.23	15.62
d-MAPI-IEA	3.49E-5	0.57	6.20	0.30	2.20	0.13	15.14

We also conducted TRPL measurements on the films deposited on FTO/c-TiO_2/m-TiO_2 substrates. Decay curves are presented in **Figure 6**. All the curves were fitted with a triple exponential function in order to obtain the best coefficient R^2 parameter. The function used and the fitting parameters extracted are gathered in **Table 1**. This allowed us to extract τ_{fast} and τ_{slow}, which represent the non-radiative recombination at the ETL/PVK interface (reflecting the speed of charge injection in the oxide transport layer) and the bimolecular recombination in the bulk of the perovskite (reflecting the bulk trap density), respectively. A higher τ_{slow} means a better bulk structural quality of the perovskite. In the meantime, a lower τ_{fast} value indicates a better charge extraction at ETL/PVK layer, therefore lower interface recombination centers

Please cite this paper as : T. Pauporté, L. Gollino, N. Mercier, Ethylammonium (IEA+)-based lead- and iodide- deficient halide perovskites (d-HPs) for solar cells. Proc. SPIE, 12422 (2023) 124220M. https://doi.org/10.1117/12.2647859

and defect density. In one hand, d-MAPI-IEA film exibited a higher τ_{fast} value than $MAPbI_3$ (6.20 ns vs 0.72 ns) which indicates a lower quality of the TiO_2/PVK interface caused by the presence of IEA^+ cations and implies a higher recombination centres density that will limit the short-circuit current density (J_{SC}) and Fill Factor (*FF*) of the final PSCs. It also implies a slower electron injection that will aggravate the hysteresis (*HI*) phenomenon. On the other hand, d-MAPI-IEA exhibits a slightly lower τ_{slow} value than $MAPbI_3$ (15.14 ns versus 15.62 ns), emphasizing a slight downgrading of the structural quality of the perovskite caused by IEA^+ insertion into the lattice. This less quality bulk perovskite is consistent with the morphology observed by SEM and the diffractograms obtained by XRD previously.

Once d-MAPI-IEA was proved to be a d-HP and fully characterized as thin films, we explored its potential for an application in PSCs by conducting *J-V* measurements. d-MAPI-IEA devices reached a maximum power conversion efficiency (PCE) of 9.54 % on reverse scan, with V_{OC} = 1.01 V, J_{SC} = 17.21 mA/cm², *FF* = 54.80 % and *HI* = 51.0 % (*PCE* = 4.67 % in forward scan). As a comparison, its analogue classic $MAPbI_3$ delivered a maximum efficiency of 18.94 %, with V_{OC} = 1.04 V, J_{SC} = 22.29 mA/cm², *FF* = 81.44 % and a hysteresis of 14.5 % (*PCE* = 16.20 % in forward scan) (**Table 2**). Associated *J-V* curves are shown in **Figure 7a**. Box charts of statistical *J-V* parameters values of $MAPbI_3$ and d-MAPI-IEA are displayed in **Figure 7b-f**. Such efficiencies were expected and can be explained by the less ETL/PVK interface quality as well as less XRD characteristics and morphology. The system also suffers from an important hysteresis. However, this issue is shared by all the d-HPs studied. Despite low PCE values, the feasibility of d-MAPI-IEA-based PSCs has been proved.

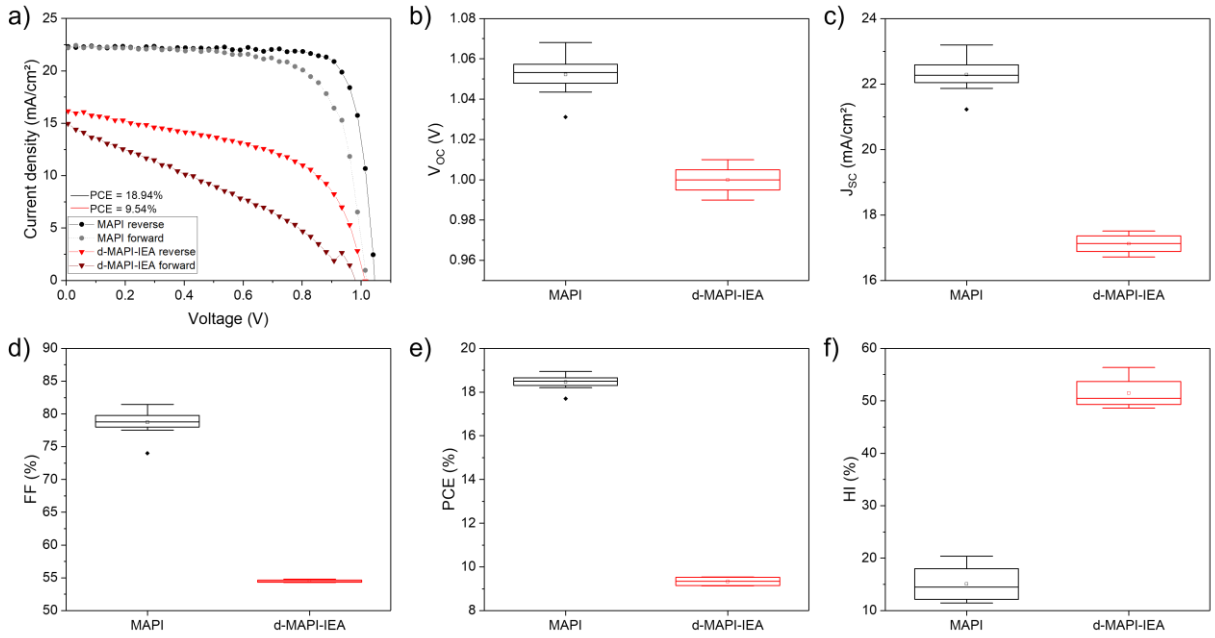

Figure 7: (a) *J-V* curves of best $MAPbI_3$ and d-MAPI-IEA devices with measured reverse scan PCEs. (b-f) Box charts of $MAPbI_3$ and d-MAPI-IEA PSCs *J-V* parameters, *PCE* and *HI*.

Table 2: Best $MAPbI_3$ and d-MAPI-IEA cells *J-V* curve parameters, PCE, and HI.

Cell	Scan direction	V_{OC} (V)	J_{SC} (mA.cm^{-2})	FF (%)	PCE (%)	HI (%)
$MAPbI_3$	Reverse	1.04	22.29	81.44	18.94	14.5
	Forward	1.02	22.33	71.29	16.20	

Please cite this paper as : T. Pauporté, L. Gollino, N. Mercier, Ethylammonium (IEA+)-based lead- and iodide- deficient halide perovskites (d-HPs) for solar cells. Proc. SPIE, 12422 (2023) 124220M. https://doi.org/10.1117/12.2647859

d-MAPI-IEA	Reverse	1.01	17.21	54.80	9.54	51.0
	Forward	0.98	15.11	31.67	4.67	

4. CONCLUSION

In the present paper, we report the successful synthesis of a new d-HP based on the use of the iodoethylammonium (IEA^+) organic cation. Lead -and iodide- deficient d-MAPI-IEA has been fabricated. The use of this perovskite in PSCs has been proven feasible. However, after diverse characterizations, d-MAPI-IEA has been found to display a downgraded structural quality along with a lower quality of the oxide ETL/PVK interface which limit its potential. Nevertheless, we believe that the replacement of the TiO_2 oxide layers on which was deposited d-MAPI-IEA by other oxide ETL such as SnO_2 or ZnO maybe be useful and revive the interest of this perovskite.

REFERENCES

[1] Lee, M. M., Teuscher, J., Miyasaka, T., Murakami, T. N. and Snaith, H. J., "Efficient Hybrid Solar Cells Based on Meso-Superstructured Organometal Halide Perovskites," Science 338, 643–647 (2012).
[2] Chung, I., Lee, B., He, J., Chang, R. P. H. and Kanatzidis, M. G., "All-solid-state dye-sensitized solar cells with high efficiency," Nature 485, 486–489 (2012).
[3] Kim, H.-S., Lee, C.-R., Im, J.-H., Lee, K.-B., Moehl, T., Marchioro, A., Moon, S.-J., Humphry-Baker, R., Yum, J.-H., Moser, J. E., Grätzel, M. and Park, N.-G., "Lead Iodide Perovskite Sensitized All-Solid-State Submicron Thin Film Mesoscopic Solar Cell with Efficiency Exceeding 9%," Sci. Rep. 2(1), 591 (2012).
[4] Chen, Z., Wang, J. J., Ren, Y., Yu, C. and Shum, K., "Schottky solar cells based on $CsSnI_3$ thin-films," Appl. Phys. Lett. 101(9), 093901 (2012).
[5] Wang, H.-Q., Wang, S., Chen, L., Yin, Z., Mei, S., Zhong, Y., Yao, Y., Li, N., Wang, J. and Song, W., "Understanding degradation mechanisms of perovskite solar cells due to electrochemical metallization effect," Sol. Energy Mater. Sol. Cells 230, 111278 (2021).
[6] Sutton, R. J., Eperon, G. E., Miranda, L., Parrott, E. S., Kamino, B. A., Patel, J. B., Hörantner, M. T., Johnston, M. B., Haghighirad, A. A., Moore, D. T. and Snaith, H. J., "Bandgap-Tunable Cesium Lead Halide Perovskites with High Thermal Stability for Efficient Solar Cells," Adv. Energy Mater. 6(8), 1502458 (2016).
[7] Leyden, M. R., Terakawa, S., Matsushima, T., Ruan, S., Goushi, K., Auffray, M., Sandanayaka, A. S. D., Qin, C., Bencheikh, F. and Adachi, C., "Distributed Feedback Lasers and Light-Emitting Diodes Using 1-Naphthylmethylamnonium Low-Dimensional Perovskite," ACS Photonics 6(2), 460–466 (2019).
[8] Wei, Y., Cheng, Z. and Lin, J., "An overview on enhancing the stability of lead halide perovskite quantum dots and their applications in phosphor-converted LEDs," Chem. Soc. Rev. 48(1), 310–350 (2019).
[9] Miao, J. and Zhang, F., "Recent progress on highly sensitive perovskite photodetectors," J. Mater. Chem. C 7(7), 1741–1791 (2019).
[10] Wang, H. and Kim, D. H., "Perovskite-based photodetectors: materials and devices," Chem. Soc. Rev. 46(17), 5204–5236 (2017).
[11] Mykhaylyk, V. B., Kraus, H. and Saliba, M., "Bright and fast scintillation of organolead perovskite MAPbBr 3 at low temperatures," Mater. Horizons 6(8), 1740–1747 (2019).
[12] Viana, B., Pauporte, T., Wang, P., Ulfa, M. and Shao, Z., "Oxide hole blocking selective contacts in perovskite solar cells," Proc. SPIE 10533, 105332 (2018).
[13] Zhu, T., Zheng, D., Liu, J., Coolen, L. and Pauporté, T., "PEAI-Based Interfacial Layer for High-Efficiency and Stable Solar Cells Based on a MACl-Mediated Grown $FA_{0.94}MA_{0.06}PbI_3$ Perovskite," ACS Appl. Mater. Interfaces 12(33), 37197–37207 (2020).
[14] Zheng, D., Chen, F., Rager, M., Gollino, L., Zhang, B. and Pauporté, T., "What are Methylammonium and Solvent Fates upon Halide Perovskite Thin-Film Preparation and Thermal Aging?," Adv. Mater. Interfaces 2201436, 2201436 (2022).

Please cite this paper as : T. Pauporté, L. Gollino, N. Mercier, Ethylammonium (IEA+)-based lead- and iodide- deficient halide perovskites (d-HPs) for solar cells. Proc. SPIE, 12422 (2023) 124220M. https://doi.org/10.1117/12.2647859

[15] Zheng, D., Zhu, T., Yan, Y. and Pauporté, T., "Controlling the Formation Process of Methylammonium-Free Halide Perovskite Films for a Homogeneous Incorporation of Alkali Metal Cations Beneficial to Solar Cell Performance," Adv. Energy Mater. 12(13), 2103618 (2022).

[16] Cao, J., Loi, H., Xu, Y., Guo, X., Wang, N., Liu, C., Wang, T., Cheng, H., Zhu, Y., Li, M. G., Wong, W. and Yan, F., "High-Performance Tin–Lead Mixed-Perovskite Solar Cells with Vertical Compositional Gradient," Adv. Mater. 34(6), 2107729 (2022).

[17] Liu, Z., Liu, P., Li, M., He, T., Liu, T., Yu, L. and Yuan, M., "Efficient and Stable FA-Rich Perovskite Photovoltaics: From Material Properties to Device Optimization," Adv. Energy Mater. 12(18), 2200111 (2022).

[18] Min, H., Lee, D. Y., Kim, J., Kim, G., Lee, K. S., Kim, J., Paik, M. J., Kim, Y. K., Kim, K. S., Kim, M. G., Shin, T. J. and Il Seok, S., "Perovskite solar cells with atomically coherent interlayers on SnO_2 electrodes," Nature 598, 444–450 (2021).

[19] Haase, F., Hollemann, C., Schäfer, S., Merkle, A., Rienäcker, M., Krügener, J., Brendel, R. and Peibst, R., "Laser contact openings for local poly-Si-metal contacts enabling 26.1%-efficient POLO-IBC solar cells," Sol. Energy Mater. Sol. Cells 186, 184–193 (2018).

[20] Yang, M., Zhang, T., Schulz, P., Li, Z., Li, G., Kim, D. H., Guo, N., Berry, J. J., Zhu, K. and Zhao, Y., "Facile fabrication of large-grain $CH_3NH_3PbI_{3-x}Br_x$ films for high-efficiency solar cells via CH_3NH_3Br-selective Ostwald ripening," Nat. Commun. 7(1), 12305 (2016).

[21] Saliba, M., Matsui, T., Domanski, K., Seo, J.-Y., Ummadisingu, A., Zakeeruddin, S. M., Correa-Baena, J.-P., Tress, W. R., Abate, A., Hagfeldt, A. and Grätzel, M., "Incorporation of rubidium cations into perovskite solar cells improves photovoltaic performance," Science 354, 206–209 (2016).

[22] Turren-Cruz, S.-H., Hagfeldt, A. and Saliba, M., "Methylammonium-free, high-performance, and stable perovskite solar cells on a planar architecture," Science 362, 449–453 (2018).

[23] Abate, A., "Perovskite Solar Cells Go Lead Free," Joule 1(4), 659–664 (2017).

[24] Zhu, Z., Jiang, X., Yu, D., Yu, N., Ning, Z. and Mi, Q., "Smooth and Compact $FASnI_3$ Films for Lead-Free Perovskite Solar Cells with over 14% Efficiency," ACS Energy Lett. 7(6), 2079–2083 (2022).

[25] Lin, R., Xu, J., Wei, M., Wang, Y., Qin, Z., Liu, Z., Wu, J., Xiao, K., Chen, B., Park, S. M., Chen, G., Atapattu, H. R., Graham, K. R., Xu, J., Zhu, J., Li, L., Zhang, C., Sargent, E. H. and Tan, H., "All-perovskite tandem solar cells with improved grain surface passivation," Nature 603, 73–78 (2022).

[26] Gollino, L. and Pauporté, T., "Lead-Less Halide Perovskite Solar Cells," Sol. RRL 5(3), 2000616 (2021).

[27] Leblanc, A., Mercier, N., Allain, M., Dittmer, J., Fernandez, V. and Pauporté, T., "Lead- and Iodide-Deficient $(CH_3NH_3)PbI_3$ (d-MAPI): The Bridge between 2D and 3D Hybrid Perovskites," Angew. Chemie Int. Ed. 56(50), 16067-16072 (2017).

[28] Leblanc, A., Mercier, N., Allain, M., Dittmer, J., Pauporté, T., Fernandez, V., Boucher, F., Kepenekian, M. and Katan, C., "Enhanced Stability and Band Gap Tuning of α-$[HC(NH_2)_2]PbI_3$ Hybrid Perovskite by Large Cation Integration," ACS Appl. Mater. Interfaces 11(23), 20743–20751 (2019).

[29] Zheng, D., Raffin, F., Volovitch, P. and Pauporté, T., "Control of perovskite film crystallization and growth direction to target homogeneous monolithic structures," Nat. Commun. 13(1), 6655 (2022).

[30] Zheng, D. and Pauporté, T., "Control of the quality and homogeneity of halide perovskites by mixed-chloride additives upon the film formation process," J. Mater. Chem. A 9(33), 17801–17811 (2021).